HHS Public Access

Author manuscript

Magn Reson Med. Author manuscript; available in PMC 2023 March 30.

Published in final edited form as:

Magn Reson Med. 2022 May ; 87(5): 2271–2286. doi:10.1002/mrm.29131.

Repeatability and Robustness of MP-GRASP T1 Mapping

Zhitao Li[1], **Xiang Xu**[2], **Yang Yang**[2], **Li Feng**[2]

[1]Department of Radiology, Stanford University, Palo Alto, California, United States

[2]Biomedical Engineering and Imaging Institute and Department of Radiology, Icahn School of Medicine at Mount Sinai, New York, NY, United States

Abstract

Purpose: To demonstrate the repeatability of fast 3D T1 mapping using MP-GRASP (Magnetization-Prepared Golden-angle RAdial Sparse Parallel) MRI and its robustness to variation of imaging parameters including flip angle in phantoms and the brain.

Methods: Multiple imaging experiments were performed to (1) assess the robustness of MP-GRASP T1 mapping to B1 inhomogeneity using a single tube phantom filled with uniform $MnCl_2$ liquid, (2) compare the repeatability of T1 mapping between MP-GRASP and IR-SE (over 12 scans) using a commercial T1MES phantom, (3) evaluate the longitudinal variation of T1 estimation using MP-GRASP with varying imaging parameters, including spatial resolution, flip angle, TR/TE, and acceleration rate, using the T1MES phantom (106 scans performed over a period of 12 months), and (4) evaluate the variation of T1 estimation using MP-GRASP with varying imaging parameters in the brain (24 scans in a single visit). In addition, the accuracy of MP-GRASP T1 mapping was also validated against IR-SE by performing linear correlation and calculating the Lin's Concordance Correlation Coefficient (CCC).

Results: MP-GRASP demonstrates good robustness to B1 inhomogeneity, with intra-slice variability below 1% in the single tube phantom experiment. The longitudinal variability is also good both in the phantom (below 2.5%) and in the brain (below 2%) with varying imaging parameters. The T1 values estimated from MP-GRASP are accurate compared to that from the IR-SE imaging (R^2=0.997, Lin's CCC=0.996).

Conclusion: MP-GRASP shows excellent repeatability of T1 estimation over time, and it is also robust to variation of different imaging parameters evaluated in this study.

Introduction

Quantitative measurement of the MR spin-lattice relaxation time (T1), known as T1 mapping, has been increasingly used in the clinic for disease characterization and follow-ups (1–6). It provides quantitative information that could serve as an image biomarker for various diseases. For example, studies have shown that T1 change is associated with

Address correspondence to: Li Feng, PhD, Biomedical Engineering and Imaging Institute, Department of Radiology, Icahn School of Medicine at Mount Sinai, 1470 Madison Ave, New York, NY, USA 10029, lifeng.mri@gmail.com.

DISCLOSURE

Li Feng is a co-inventor in a patent (Patent number 9921285) on the GRASP imaging technique.

neurological disorders in the brain (6,7). In carotid plaque studies, T1 mapping of the carotid atherosclerosis has been used to characterize plaque compositions (8). In patients with myocardial infarction, the change of T1 in the myocardial wall has been used to identify scars in follow-up exams (1,9). For abdominal imaging, T1 mapping of the liver can be used to characterize cirrhotic liver tissues (10,11) and to identify potential tumor malignancy (12), and T1 can also be used as an image marker for diagnosing declining kidney function (13). In addition, acquisition of native T1 (T1 values measured before injection of a contrast agent) is desired to convert dynamic MR signal to contrast concentration in the quantification of dynamic contrast-enhanced MR perfusion to achieve more accurate and reliable pharmacokinetic analysis (14).

Currently, commonly used clinical T1 mapping methods can roughly be classified into two categories. First, T1 maps can be quickly acquired with a fast gradient echo (GRE) sequence that is played out with varying flip angles, known as the VFA (variable flip angle) method (15,16). For example, DESPOT1 (Driven equilibrium single pulse observation of T1) is a rapid and widely-accepted 3D VFA T1 mapping technique (17) that has been used in clinical exams, and it can be implemented with two flip angles only. However, T1 fitting using the VFA method relies on accurate flip angle information, making this method particularly sensitive to B1 field inhomogeneity. As a result, the VFA method typically requires an additional step for B1 calibration/mapping, which complicates this imaging method (18). The second type of T1 mapping method implements magnetization preparation pulses, such as inversion recovery (IR) or saturation recovery (SR), to capture information on T1 recovery using a fast-imaging sequence. In particular, IR preparation has been commonly combined with fast GRE acquisition with a fixed small flip angle to generate T1 maps (19,20). This acquisition scheme, known as Look-Locker imaging, has much improved robustness to B1 inhomogeneity (19,20). However, the Look-Locker method typically requires longer scan time, particularly for 3D acquisition, due to the need to acquire multiple images at different inversion times (TIs). The acquisition after each IR preparation can also be performed intermittently to shorten scan time. For example, MP2RAGE is a method getting increasing attention for both qualitative and quantitative applications. After the IR preparation, it acquires images at two different TIs, which can then be used to generate a T1 map. The VFA and Look-Locker acquisition can also be combined. For example, MR fingerprinting (MRF) (21) combines the features of VFA and Look-Locker imaging with a dictionary matching algorithm. This allows for simultaneous mapping of multiple image parameters (such as T1 and T2) efficiently with a synergistic imaging paradigm. However, since the MRF implements VFA acquisition, knowledge of B1 is also essential (22,23).

During the past years, different fast imaging methods have been developed to accelerate T1 mapping based on the VFA or the Look-Locker acquisition scheme (24–35). These methods use advanced reconstruction strategies, such as compressed sensing, low-rank methods, model-based methods, deep learning techniques, or a combination of them to reconstruct dynamic T1-weighted images or T1 maps directly from undersampled measurements, and they have all demonstrated promising results. However, majority of the efforts in this area have been focused on technical development, optimization, and clinical evaluation. The longitudinal repeatability of T1 estimation, as a very important

question for any new T1 mapping methods, has been less studied. While many studies intended to evaluate the repeatability of new T1 mapping methods, this is usually assessed in a limited number of experiments, and there are very limited studies to rigorously evaluate the T1 mapping repeatability with varying imaging parameters over a long period. Recently, a rapid 3D T1 mapping technique, called MP-GRASP (Magnetization Prepared Golden-angle RAdial Sparse Parallel) MRI, has been proposed (36). MP-GRASP enables fast 3D Look-Locker T1 mapping combining accelerated stack-of-stars radial acquisition with subspace-constrained sparse image reconstruction. While the initial performance of this technique has been previously evaluated and validated both in phantom and in vivo, the longitudinal performance of this technique, as an important question, remains to be investigated. The main contribution of this work was first to summarize the conditions under which Look-Locker T1 mapping can be robust to B1 inhomogeneity. We then sought to evaluate the repeatability and robustness of MP-GRASP in a phantom over a period of ~12 months with varying imaging parameters, including spatial resolution, flip angle, repetition time (TR), echo time (TE), acceleration rate/total scan time, imaging bandwidth and coil elements. Such experiments were also repeated in one volunteer for in-vivo demonstration. With these rigorously designed experiments, we sought to validate the hypothesis that T1 mapping using MP-GRASP is repeatable and is robust towards variation of different imaging parameters and B1 inhomogeneity at the same field strength.

Theory

In this section, we first review the GRE-based Look-Locker T1 mapping method (the acquisition scheme that MP-GRASP is based on) and illustrate the conditions under which this type of method can be robust to flip angle variation (and effectively B1 inhomogeneity). We then review additional correction that is needed to account for the relaxation effect during spoiling after IR preparation, which is important for estimation of more accurate T1 values in Look-Locker imaging.

B1 Robustness of Look-Locker T1 mapping

The signal evolution of the Look-Locker T1 mapping method can be expressed as the following equation (19):

$$M(t) = M_{ss} - (M + M_{ss})e^{-\frac{t}{T_1^*}} \quad [1]$$

As shown in Figure 1a, $-M$ is the magnetization immediately before the first RF excitation in GRE acquisition, M_{ss} is the magnetization after the signal achieves steady state with a small and constant flip angle ($\alpha°$) following the IR preparation. T_1^* represents the effective T1 value when an RF pulse is constantly applied for data acquisition, and it is given by the following equation (19):

$$T_1^* = \left[\frac{1}{T_1} - \left(\frac{1}{TR}\right)ln(cos\,\alpha)\right]^{-1} \quad [2]$$

With a small flip angle, a valid assumption of $TR \ll T_1^* < T_1$ and ignoring T2* decay, Equation.1 can be reformatted as the following three-parameter equation:

$$M(t) = A - Be^{-\frac{t}{T_1^*}} \quad [3]$$

where

$$A = M_{ss} = \frac{M_0\left(1 - e^{-TR/T_1}\right)}{1 - cos\,\alpha\, e^{-TR/T_1}} = \frac{M_0\left(1 - e^{-TR/T_1}\right)}{1 - e^{-TR/T_1^*}} \approx M_0\frac{T_1^*}{T_1} \quad [4]$$

$$B = M + M_{ss} = M + M_0\frac{T_1^*}{T_1} \quad [5]$$

When $M = M_0$, Equation. 5 can be revised as

$$B = M_0\left(1 + \frac{T_1^*}{T_1}\right) \quad [6]$$

Thus, once the three unknown parameters, A, B and T_1^*, are fitted following Equation 3, T1 can then be generated using the following equation (19):

$$T_1 = T_1^*\left(\frac{B}{A} - 1\right) \quad [7]$$

Equations 3 and 7 suggest that T1 estimation in Look-Locker imaging does not require the knowledge of flip angle and other imaging parameters when $TR \ll T_1^* < T_1$ and $M = M_0$ (19). Thus, it can be robust to flip angle variation (and effectively B1 inhomogeneity). This is an important and highly-desired feature in quantitative MRI. The first condition ($TR \ll T_1^* < T_1$) can be achieved by using a fast-imaging sequence (e.g., GRE), and the second condition ($M = M_0$) can be achieved when (a) the magnetization before each IR preparation is at equilibrium (M_0), (b) accurate IR excitation is implemented, and (c) there is no delay between the end of IR preparation and the first RF excitation (to avoid T1 recovery before the first k-space measurement). The requirement (a) can be fulfilled by adding a sufficient delay between consecutive IR preparations to allow for full magnetization recovery, as shown in Figure 1b. The requirement (b) can be fulfilled using a carefully designed adiabatic IR pulse in practice. The requirement (c) is challenging at the first look, since a spoiler is typically needed right after each IR excitation pulse, thus generating a gap during which T1 recovery occurs. Fortunately, this can be corrected in practical implementation as will be described in the following subsection, and it does not affect the imaging performance of Look-Locker T1 mapping. The overall robustness of Look-Locker T1 mapping to flip angle variation makes it attractive towards routine clinical use, particularly for longitudinal imaging studies. However, it should be noted that a small flip angle is preferred in Look-Locker, as described in (19) and validated in our imaging experiments later.

Correction for Relaxation Effect During Post-IR Spoiling

In practical implementation of Look-Locker T1 mapping, it is hard to acquire the true M_0 signal even with an adiabatic IR pulse. This is because a typical implementation of an IR module requires a spoiler after the IR preparation to destroy any residual signal coming from spins, in case they are not been fully inverted (Figure 1a). The spoiler is usually in the scale of a few milliseconds and adds a time interval (denoted as Δt) between the end of IR preparation and the first k-space measurement. During this time interval, the spins start magnetization recovery, thus preventing the acquisition of the true M_0 signal. Based on a prior study (37), the actual initial magnetization state right before the first k-space measurement, denoted as $M_0^{'}$, can be expressed as follows:

$$M_0^{'} = M_0 - 2M_0 e^{-\frac{\Delta t}{T_1}} \approx M_0\left(1 - 2\frac{\Delta t}{T_1}\right) \quad [8]$$

The fitted T1, denoted as $T_1^{'}$, can then be derived following Equation 4 as:

$$T_1^{'} = \frac{M_0^{'}}{M_{ss}} T_1^{*} = \frac{M_0^{'}}{M_0} T_1 = T_1 - 2\Delta t \quad [9]$$

As a result, the fitted $T_1^{'}$ needs to be corrected by adding $2\Delta t$ to derive the final T1 value.

Methods

Following the above theoretical description, we designed multiple imaging experiments (both in phantoms and in-vivo) to verify that MP-GRASP enables fast and accurate 3D T1 with robustness to variation of different imaging parameters and B1 inhomogeneity in practical implementation.

Recap of MP-GRASP Acquisition and Reconstruction

MP-GRASP is a Look-Locker-type T1 mapping method that enables accelerated 3D T1 mapping. The MP-GRASP acquisition combines IR preparation with stack-of-stars radial imaging, as illustrated in Figure 1b. The IR excitation was implemented using an adiabatic pulse to ensure an accurate 180° excitation. Following each IR preparation, a series of radial stacks are acquired, with an order that all spokes (or all partitions) at a given rotation angle are acquired before moving to the next rotation angle. For a given radial stack with the same acquisition angle, different partitions can be acquired in a linear reordering or center-out reordering scheme, as shown in Figure 1c. As described in the theory section, a delay is added between different IR preparations to allow for sufficient magnetization recovery. The rotation angle of radial stacks follows the equation shown in Figure 1b, where two variables m and n indicate the m^{th} spoke in the n^{th} repetition, and N indicates the total number of repetitions to be acquired. As shown in our MP-GRASP presentation (36), this ensures that after synchronizing all repetitions, radial spokes for a given TI can achieve a uniform k-space coverage. In the MP-GRASP acquisition, the TR is defined as the time between consecutive α° RF pulses. Many parameters, such as the number of partitions, the total

number of repetitions, the number of stacks in each repetition and the delay time, can all be pre-defined.

The MP-GRASP reconstruction employs a subspace-constrained sparse reconstruction algorithm. Specifically, temporal basis functions are first estimated from a T1 relaxation dictionary obtained by solving the Bloch equations. The temporal basis functions are then used to generate a subspace, which can represent the entire T1 image series with only a few dominant principal coefficients. This helps reduce the number of unknown and thus the degrees of freedom in image reconstruction, leading to increased reconstruction quality over standard compressed sensing reconstruction (38). In addition, self-calibrating GRAPPA (GeneRalized Autocalibrating Partial Parallel Acquisition) operator gridding was included in MP-GRASP to increase image reconstruction speed (39,40). More details about MP-GRASP reconstruction can be found in (36). After reconstruction of a T1 mapping image series, T1 maps can then be estimated following the three-parameter model outlined in Equations 3 and 7, and additional correction can be made following Equation 9.

Experimental Design

Two different phantoms were prepared for our imaging experiments. The first phantom was made in our lab. It has a single container that is filled with uniform $MnCl_2$ liquid, as shown in Figure 2a. The phantom has a diameter of 12 centimeters and a height of 13 centimeters. This is referred to as single tube phantom hereafter. With this design, the phantom is supposed to have homogeneous T1 value in each spatial location, and thus it is ideal to validate the influence of B1 inhomogeneity. The second phantom was selected as the T1MES phantom (41), which is a fully validated commercial phantom that consists of 9 vials of samples immersed inside a large container. The T1 value of the 9 vials is from ~300 ms to ~1400 ms, which is a range that represents the T1 values of most organ/tissue of interest in human. To minimize the influence of temperature on T1 values, the phantom was put inside the cabinet of the scanner room all the time. All imaging experiments were performed on a 3T MRI scanner (MAGNETOM Skyra, Siemens Healthcare GmbH, Germany).

Using these two phantoms, five experiments were designed to validate the robustness of MP-GRASP, as summarized below.

Experiment 1: The robustness of MP-GRASP to B1 inhomogeneity was first validated using the single tube phantom. The hypothesis was that even with inhomogeneous RF excitation (a typical situation in everyday MRI exams), repeatable T1 values are still expected in all pixels of the acquired image, given that the phantom has a single tube with uniform liquid. In this experiment, a single-slice IR-based spin echo (IR-SE) sequence was also performed to measure gold standard T1 values and to validate the accuracy of MP-GRASP T1 mapping.

Experiment 2: The influence of flip angle and delay time between consecutive IR preparations (see Figure 1b) on T1 estimation was investigated using the single tube phantom.

Experiment 3: The repeatability of both MP-GRASP and IR-SE T1 mapping was compared using the T1MES phantom. For this purpose, both MP-GRASP and IR-SE were scanned 12 times. The accuracy of MP-GRASP T1 mapping was also validated against IR-SE T1 mapping again in T1MES phantom.

Experiment 4: The longitudinal variation of T1 estimation using MP-GRASP was investigated using the T1MES phantom. In total, MP-GRASP T1 mapping was performed on 106 occasions over a period of ~12 months in the T1MES phantom with varying imaging parameters.

Experiment 5: Finally, the repeatability of MP-GRASP T1 mapping in the brain was studied in a healthy volunteer with varying imaging parameters. MP-GRASP T1 mapping was performed 24 times in a single visit.

Imaging Experiments

Experiment 1: The single tube phantom was scanned using MP-GRASP with the following imaging parameters: FOV=256×256 mm^2, matrix size=256×256, voxel size = 1×1 mm^2, flip angle=5°, TR/TE=3.31/1.56 ms, total repetitions=21, slice thickness=3 mm, total number of slices=32, and total scan time=3.35 min. A 6-second delay time was inserted between different IR preparations, and 75% partial Fourier was applied along the partition dimension. The number of stacks (number of radial rotations) after each IR preparation=48, resulting 48 acquired TIs with a step size of 79.44 (TR×32*0.75) ms. Single-slice 2D B1 maps, (one in axial plane and one in coronal plane) were acquired in to assess the B1 variation, and the B1 maps were not used in the generation of T1 values in our method. B1 mapping was performed using a method as described by Chung et al (42).

For comparison, the single tube phantom was also scanned using IR-SE (one slice only) with the following parameters: FOV = 256×256 mm^2, matrix size = 256×256, voxel size = 1×1 mm^2, flip angle = 90°−180°, slice thickness = 5 mm, TE = 15 ms, TR = 10000 ms. 12 images were acquired at inversion delay times (TI) of 30, 50, 100, 200, 300, 400, 500, 700, 1000, 1500, 2000 and 3000 ms. The total acquisition time was ~8 hours.

Three slices of MP-GRASP T1 map corresponding to different slice locations (see Figure 2b) were selected for analysis. For each slice, a large circular region of interest (ROI) was manually placed on the T1 map to calculate corresponding mean T1 values and standard deviation. The same analysis was also performed on the IR-SE T1 map. The intra-slice variability (as an indicator or repeatability) for each images slice, defined as the coefficient of variation (the ratio of standard deviation over the mean T1 value), was then compared. This definition of repeatability was also applied to the following experiments.

Experiment 2: MP-GRASP T1 mapping was performed on the single tube phantom to investigate the influence of flip angle and delay time on T1 estimation. Based on the protocol used in Experiment 1, MP-GRASP was performed with a flip angle of 1°, 3°, 5°, 8°, 12°, 20° and 30° in the first setting (other parameters were not changed). In the second setting, MP-GRASP was performed with a delay time of 0s, 1s, 3s, 6s (other parameters

were not changed). Similar to Experiment 1, the mean T1 value, the standard deviation and the intra-slice variability were calculated from a central slice T1 map for comparison.

Experiment 3: The T1MES phantom was scanned using both MP-GRASP and IR-SE for a total of 12 times each in two settings using the protocol as in Experiment 1. In each setting, the phantom was put inside the scanner all the time. The time/gap between the two settings was 4 days, and the phantom was put back to the cabinet of the scanner room during this time. In the first setting, MR scans started 3 hours after the phantom was put into the scanner. MP-GRASP and IR-SE were alternatively scanned for a total of 8 times each (referred to as Scan 1 to Scan 8 hereafter). For each pair of scans, MP-GRASP was always performed before IR-SE. In the second setting, MRI scans started right after the phantom was put into the scanner. Same as the first setting, MP-GRASP and IR-SE were alternatively scanned for a total of 4 times each (referred to as Scan 9 to Scan 12 hereafter). As a result, both MP-GRASP and IR-SE were scanned for a total of 12 times each.

After image reconstruction and T1 map generation, ROIs were manually placed for each phantom vial in the MP-GRASP and IR-SE T1 maps from all the scans. For MP-GRASP, a central slice T1 map (with matching slice location to IR-SE) was used. The repeatability of T1 estimation was then compared between MP-GRASP and IR-SE over all the 12 scans. In addition, the T1 values from the two types of methods were averaged through all the 12 scans for comparison using linear correlation and Lin's concordance correlation coefficient (CCC) (43).

Experiment 4: The T1MES phantom was scanned for a total of 106 times over a period of ~12 months. Different imaging parameters, including the spatial resolution, flip angle, TR/TE, bandwidth, coil elements, total number of repetitions (related to acceleration rate and total acquisition time), and the kz reordering scheme, were varied from scan to scan. The varying imaging parameters for all the 106 scans are summarized in Supporting Information Table S1. Specifically, these datasets were acquired at different time points after the phantom was put into the scanner. For example, some datasets were acquired right after the phantom was put into the scanner while some datasets were acquired several hours after the phantom was put into the scanner. This could cause temperature-induced T1 changes, which were taken into specific consideration when summarizing the results later. After image reconstruction and T1 map generation, ROIs were manually placed for each vial in the MP-GRASP T1 maps from all the 106 scans. The longitudinal variation of T1 estimation and corresponding repeatability in each phantom vial were assessed for a central slice and a peripheral slice.

Experiment 5: MP-GRASP T1 mapping was performed in a healthy volunteer (male, age=30). The human imaging study is HIPAA-compliant and was approved by the local Institutional Review Board (IRB). Written informed consent was obtained from the volunteer before the MR scans. A total of 24 scans were performed with varying imaging parameters in a single visit. A 32-element head coil array was used for the first 12 protocols and a 12-element head coil array was used in the next 12 protocols. The volunteer was given a short break outside the scanner room when changing the coil setup, and the subject was

repositioned for the second part. All the imaging parameters are summarized in Supporting Information Table S2.

After image reconstruction and T1 map generation, a total of 9 ROIs were placed on each dataset, including 5 ROIs in the white matters, 2 ROIs in the caudate and 2 ROIs in the thalamus. ROIs were manually placed on matching locations in all the datasets. Due to varying spatial resolution, the gray matter was not included for analysis to avoid partial volume effect. The repeatability of mean T1 value in all the datasets was assessed for each ROI.

Results

All the imaging experiments were successfully performed, and all the datasets were reconstructed to generate T1 maps. The results are summarized for each experiment.

Experiment 1:

The B1 maps for the single tube phantom imaging are shown in Figure 2b, including one axial slice and one coronal slice. The maps were acquired to show inhomogeneous excitation only and were not used for image reconstruction or T1 estimation. The arrows indicate the slice locations used for subsequent image analysis. As can be seen from the B1 maps, there is B1 inhomogeneity along different orientations. Figure 2c compares the T1 map estimated from IR-SE with T1 maps in different slice locations estimated from MP-GRASP. All the T1 maps are homogeneous in general, indicating that both methods can be robust to B1 variation. The quantitative results shown in Figure 2d further validate this observation. MP-GRASP generated mean T1 values that are consistent with the IR-SE measurement. Although the IR-SE T1 map has a lower standard deviation compared to MP-GRASP, both methods yielded very low intra-slice variation (below 1%), indicating high repeatability.

Experiment 2:

Figure 3a compares MP-GRASP T1 maps with different flip angles. The results suggest that consistent mean T1 values can be obtained with different flip angles up to 20° for the target T1 value in our single tube phantom. It should be noted that the variation of flip angle here is effectively similar to the variation of B1, although they are not identical. This further validated the observation in Experiment 1 that MP-GRASP can be robust to B1 variation. The mean T1 value estimated from flip angle of 1° is noisy because of the low signal. The standard deviation and intra-slice variability in Figure 3b indicate that the T1 map from the flip angle of 5° has the lowest intra-slice variation. This can be attributed to the fact that the Ernst angle is close to 5° for the target T1 and the selected TR. The deviation of MP-GRASP mean T1 values from the reference IR-SE T1 value is also shown in Figure 3b, which suggest that the mean T1 value estimated from flip angle of 30° produced errors. As shown in Figure 3c, this is because of the flattening of T1 recovery curve (loss of T1 recovery range, the light grey curve) in Look-Locker acquisition, making reliable T1 estimation impossible. These results further validate that a small flip angle is important for Look-Locker T1 mapping.

Figure 4a compares MP-GRASP T1 maps with different delay times. It can be seen that insufficient delay prevents full signal recovery before a new IR preparation, thus resulting in T1 estimation errors. A numerical simulation was performed to investigate the delay time needed for different T1 values to be estimated. It indicates that with the increase of underlying T1 values, the delay time also needs to be increased to ensure accurate T1 estimation in standard Look-Locker imaging.

Experiment 3:

Figure 5a compares one slice of T1 map estimated from IR-SE and MP-GRASP. There is a strong correlation between the mean T1 values estimated from the two methods, as shown in Figure 5b, and the Lin's CCC was 0.9962 (95% confidence interval= 0.9870 to 0.9989). The repeatability of T1 estimation over all the 12 scans is good for both IR-SE and MP-GRASP, with variation in all phantom vials below 2%.

Figure 6 plots the temporal variation of T1 values in different phantom vials for all the 12 scans. It can be seen that for each setting (Scan 1–8 and Scan 9–12), the T1 estimation is repeatable. However, for vials with larger T1 values (e.g., vial 7 to vial 9), there is a jump of measured T1 value from the first scan (Scan 1 and Scan 9) to the rest, and this trend was observed both in the IR-SE and the MP-GRASP results. This change can be attributed to the adjustment of temperature after the phantom was put inside the scanner (due to difference of temperature between scanner room cabinet and scanner itself), so it mainly affected the first scan. In addition, the T1 values estimated in the second setting (Scan 9 to Scan 12) are generally lower compared to that from the first setting (Scan 1 to Scan 8). Since this was also observed both in the IR-SE and the MP-GRASP results, it can be due to the fact that the temperature of the scanner room is not constant all the time (e.g., due to the air conditioner control and other factors). Furthermore, it was found that the influence of temperature is bigger in vials with larger T1 values compared to those with smaller T1, and this finding is consistent with that reported in the original T1MES paper (41).

Experiment 4:

The longitudinal variations of mean T1 values over all the 106 datasets are summarized for each phantom vial in Figure 7 (for the central slice), along with corresponding variation of flip angle and voxel size. Similar results for the peripheral slice are shown in Supporting Information Figure S1. Different line colors indicate plots for different phantom vials. The longitudinal variability of T1 estimation is also shown in the figure. The variation of T1 measurement was below 2% for vials 1–8, and it was slightly larger for vial 9, which is still below 2.5%. These results suggest good repeatability of T1 mapping over time. For phantom vial 8 and vial 9, there is slight increase and then decrease of mean T1 values along time, which is consistent with the trend observed in Figure 6 that could be caused by the change of temperature.

Figure 8 shows representative MP-GRASP T1 maps from the T1MES phantom at different time points. Despite different imaging parameters, the T1 maps are visually consistent for all the phantom vials.

Experiment 5:

The dynamic variations of MP-GRASP T1 values over all the 24 brain datasets are summarized in Figure 9 for all the 9 selected ROIs. The variation of T1 measurement, as shown in the figure, is below 2% in all ROIs, which suggests good repeatability of MP-GRASP T1 mapping in the brain.

One slice of brain T1 map acquired with different flip angles, acquisition times and spatial resolution are shown in Figure 10. On the top row, the T1 maps were acquired with an in-plane spatial resolution of 1.0×1.0 mm^2, flip angle of 5°, and different acquisition times/acceleration rates. For the bottom row, the T1 maps were acquired using different flip angles but the same spatial resolution (0.8×0.8 mm^2) and acquisition time. Overall, the brain T1 maps from different imaging protocols are visually consistent.

Discussion

Repeatability is one of the most important questions that all quantitative MRI techniques must evaluate before translating for clinical use, and it is highly desired that robust and repeatable quantification can be obtained. In this work, we aimed to assess the repeatability of MP-GRASP, our recently proposed 3D T1 mapping technique. We also aimed to verify that T1 mapping using MP-GRASP is independent of imaging parameters such as TR, TE, flip angle, resolution and others. In order to achieve this goal, we carefully designed five different imaging experiments using a home-made phantom and a commercial phantom. We also repeated the study in a volunteer to assess the repeatability of brain T1 mapping. Our initial results have demonstrated that MP-GRASP is highly repeatable, with well accepted repeatability (coefficient of variation) for rapid T1 mapping both in phantoms and in the brain, and it holds great potential toward ultimate routine clinical use.

The robustness to flip angle variation is an important feature of Look-Locker T1 mapping compared to other T1 mapping methods such as the VFA method (18) and more advanced multiparametric methods such as the MRF (22,23). Before the phantom and in-vivo experiments, the Look-Locker T1 mapping approach was first reviewed in this study, and we illustrated why Look-Locker imaging can be robust to flip angle variation and the conditions that need to be meet to achieve this. The main requirements include the use of an adiabatic IR pulse to ensure sufficient inversion efficiency and sufficient delay time between different IR preparations to allow for magnetization recovery. It should be noted that although flip angle variation is not identical to B1 inhomogeneity, they are effectively related.

In this study, the T1MES phantom was scanned 106 times over a period of ~12 months with varying imaging parameters. The first portion of the scans was performed in the summer of 2020, the second portion was performed between March to May in 2021, and the third portion of the scans was performed in the summer of 2021. To ensure that the underlying T1 of the phantom did not change, we used a standardized T1MES phantom with confirmed reliability (44) and a range of T1 values that are close to the T1 values observed in humans. These experiments have indicated that MP-GRASP could be reliable with a high repeatability for longitudinal follow-up study, which is highly important in assessing longitudinal disease changes. Although there were similar studies to evaluate the

repeatability of new quantitative MRI methods in phantoms before (45,46), these prior studies all used the same imaging protocol for MRI scans at all times and did not assess the influence of imaging parameters on T1 quantification.

In addition to studying the repeatability of MP-GRASP with varying imaging parameters, we have also compared the repeatability between MP-GRASP and IR-SE, the accepted gold standard method for T1 estimation. The results show that the variation pattern of T1 estimation using these two methods is consistent (Figure 6). The variation of T1 values in our study (Figure 6) can be the fact that (1) the temperature is different from the scanner room cabinet to the scanner bore, and (2) the temperature inside the scanner bore could also be varied in different days, which could be caused by the change of setting in room air conditioner and the scanner fan (a fan is typically installed inside the scanner). Therefore, to ensure more reliable phantom T1 mapping experiments, particularly measurement of larger T1 values, it is highly suggested that the phantom can be put into the scanner for 8–10 hours before the start of imaging experiments.

Our experiments with different flip angles (Figure 3) show that varying flip angles does not affect the accuracy of T1 estimation, which confirms what we summarized in the theory section above. With the three-parameter T1 fitting approach outlined in Equations 3 and 7, the information of flip angle is not needed in the fitting process. As such, MP-GRASP is robust to flip angle variation, which can effectively be treated as B1 robustness as demonstrated in Figure 2. This is indeed one of the most important advantages of Look-Locker T1 mapping that was pointed out decades ago (19,20), and this feature can ensure good reliability in longitudinal studies of diseases, where it could be hard to guarantee the same imaging parameters for different MRI scans. Our experiments also suggested that a larger flip angle should be avoided in Look-Locker T1 mapping, because this can substantially reduce signal and also shorten the range of T1 recovery, as shown in Figure 3, thus reducing the accuracy of T1 fitting.

This study also assessed the influence of delay time on T1 fitting accuracy. Insufficient delay does not allow to acquire signal at the equilibrium state and thus prevents the use of the three-parameter model (Equations 3 and 7) to generate T1 maps. Meanwhile, a short delay between consecutive IR preparations also reduces the T1 recovery range, which can potentially lead to fitting errors. As described above, a delay period between consecutive IR preparations is required in MP-GRASP to ensure robustness to the B1 inhomogeneity. This, however, can greatly prolong total scan time. In our experiment, this delay time was set as 6 seconds, which is barely enough for T1 recovery (>99.9%) in the vial with the largest T1 value in the T1MES phantom. In practical implementation, this delay should be chosen based on the T1 of the organ or tissue to be studied. A recent study has shown that the delay can be avoided by acquiring images with two different flip angles, which allows for estimation of both a B1 map and a T1 map (47). However, while the delay can be avoided, the acquisition becomes sensitive to B1 inhomogeneity, making an accurate B1 map necessary for T1 estimation. Meanwhile, acquisition of T1 mapping images using two flip angles doubles total scan time and requires careful selection of the second flip angle.

Finally, our study has limitations that require discussion. First, different from the phantom experiments, the in-vivo experiments were performed on the same day during a single visit. This was because it was challenging to recruit a volunteer who can be committed for multiple visits. Meanwhile, in vivo study in a single visit could also avoid potential T1 changes due to normal physiological variations in the subject across diffident imaging sessions. Second, we only evaluated our method in one scanner platform and one vendor. Future works will be needed to further validate the performance of MP-GRASP across different scanner platforms.

Conclusion

This study demonstrated the good repeatability of MP-GRASP for T1 mapping over time. The method is also shown to be robust to variation of different imaging parameters such as spatial resolution, flip angle and others evaluated in this study. With fast, repeatable and reliable T1 mapping, MP-GRASP represents a promising quantitative MRI technique towards future routine clinical translation.

Supplementary Material

Refer to Web version on PubMed Central for supplementary material.

Acknowledgement

The authors thank Dewey Chu for help with the phantom experiments and thank Mahesh Keerthivasan for helpful discussion in interpret the results. The authors also thank Zidan Yu, Martijn Cloos and Ding Xia for help in making the single tube phantom. This work was supported in part by the NIH (R01 EB030549).

Grant Support:

NIH R01EB030549

References

1. Taylor AJ, Salerno M, Dharmakumar R, Jerosch-Herold M. T1 Mapping: Basic Techniques and Clinical Applications. JACC Cardiovasc. Imaging 2016;9:67–81 doi: 10.1016/J.JCMG.2015.11.005. [PubMed: 26762877]
2. Bottomley PA, Hardy CJ, Argersinger RE, Allen moore G. A review of 1H nuclear magnetic resonance relaxation in pathology: Are T1 and T2 diagnostic? Med. Phys 1987;14:1–37 doi: 10.1118/1.596111. [PubMed: 3031439]
3. Puntmann VO, Peker E, Chandrashekhar Y, Nagel E. T1 Mapping in Characterizing Myocardial Disease. Circ. Res 2016;119:277–299 doi: 10.1161/CIRCRESAHA.116.307974. [PubMed: 27390332]
4. Fontana M, Banypersad SM, Treibel TA, et al. Native T1 mapping in transthyretin amyloidosis. JACC Cardiovasc. Imaging 2014;7:157–165 doi: 10.1016/J.JCMG.2013.10.008. [PubMed: 24412190]
5. Puntmann VO, Voigt T, Chen Z, et al. Native T1 mapping in differentiation of normal myocardium from diffuse disease in hypertrophic and dilated cardiomyopathy. JACC Cardiovasc. Imaging 2013;6:475–484 doi: 10.1016/J.JCMG.2012.08.019. [PubMed: 23498674]
6. Vrenken H, Geurts JJG, Knol DL, et al. Whole-brain T1 mapping in multiple sclerosis: Global changes of normal-appearing gray and white matter. Radiology 2006;240:811–820 doi: 10.1148/radiol.2403050569. [PubMed: 16868279]

7. HB L, J F, P J, et al. Assessment of demyelination, edema, and gliosis by in vivo determination of T1 and T2 in the brain of patients with acute attack of multiple sclerosis. Magn. Reson. Med 1989;11:337–348 doi: 10.1002/MRM.1910110308. [PubMed: 2779421]
8. BF C, DH P, MI L, et al. Three-dimensional quantitative T1 and T2 mapping of the carotid artery: Sequence design and in vivo feasibility. Magn. Reson. Med 2016;75:1008–1017 doi: 10.1002/MRM.25634. [PubMed: 25920036]
9. Jellis CL, Kwon DH. Myocardial T1 mapping: modalities and clinical applications. Cardiovasc. Diagn. Ther 2014;4:126 doi: 10.3978/J.ISSN.2223-3652.2013.09.03. [PubMed: 24834410]
10. Kim KA, Park MS, Kim IS, et al. Quantitative evaluation of liver cirrhosis using T1 relaxation time with 3 tesla MRI before and after oxygen inhalation. J. Magn. Reson. Imaging 2012;36:405–410 doi: 10.1002/jmri.23620. [PubMed: 22392835]
11. Horowitz JM, Venkatesh SK, Ehman RL, et al. Evaluation of hepatic fibrosis: a review from the society of abdominal radiology disease focus panel. Abdom. Radiol 2017;42:2037–2053 doi: 10.1007/s00261-017-1211-7.
12. MA G, PF H, S S, et al. Value of T1 and T2 relaxation times from echoplanar MR imaging in the characterization of focal hepatic lesions. AJR. Am. J. Roentgenol 1993;160:1011–1017 doi: 10.2214/AJR.160.5.8470568. [PubMed: 8470568]
13. Huang Y, Sadowski EA, Artz NS, et al. Measurement and comparison of T1 relaxation times in native and transplanted kidney cortex and medulla. J. Magn. Reson. Imaging 2011;33:1241–1247 doi: 10.1002/jmri.22543. [PubMed: 21509885]
14. Fennessy FM, Fedorov A, Gupta SN, Schmidt EJ, Tempany CM, Mulkern RV. Practical considerations in T1 mapping of prostate for dynamic contrast enhancement pharmacokinetic analyses. Magn. Reson. Imaging 2012;30:1224–1233 doi: 10.1016/j.mri.2012.06.011. [PubMed: 22898681]
15. Heule R, Ganter C, Bieri O. Variable flip angle T1 mapping in the human brain with reduced t2 sensitivity using fast radiofrequency-spoiled gradient echo imaging. Magn. Reson. Med 2016;75:1413–1422 doi: 10.1002/mrm.25668. [PubMed: 25980525]
16. Cheng H-LM, Wright GA. Rapid high-resolution T1 mapping by variable flip angles: Accurate and precise measurements in the presence of radiofrequency field inhomogeneity. Magn. Reson. Med 2006;55:566–574 doi: 10.1002/MRM.20791. [PubMed: 16450365]
17. SC D TM P, BK R. High-resolution T1 and T2 mapping of the brain in a clinically acceptable time with DESPOT1 and DESPOT2. Magn. Reson. Med 2005;53:237–241 doi: 10.1002/MRM.20314. [PubMed: 15690526]
18. Schabel MC, Morrell GR. Uncertainty in T1 mapping using the variable flip angle method with two flip angles. Phys. Med. Biol 2008;54:N1 doi: 10.1088/0031-9155/54/1/N01. [PubMed: 19060359]
19. Deichmann R, Haase A. Quantification of T1 values by SNAPSHOT-FLASH NMR imaging. J. Magn. Reson 1992;96:608–612 doi: 10.1016/0022-2364(92)90347-A.
20. Deichmann R, Adolf H, Nöth U, Morrissey S, Schwarzbauer C, Haase A. Fast T2-mapping with snapshot flash imaging. Magn. Reson. Imaging 1995;13:633–639 doi: 10.1016/0730-725X(95)00004-Z. [PubMed: 7674860]
21. Ma D, Gulani V, Seiberlich N, et al. Magnetic resonance fingerprinting. Nature 2013;495:187–192 doi: 10.1038/nature11971. [PubMed: 23486058]
22. Ma D, Coppo S, Chen Y, et al. Slice profile and B1 corrections in 2D magnetic resonance fingerprinting. Magn. Reson. Med 2017;78:1781–1789 doi: 10.1002/MRM.26580. [PubMed: 28074530]
23. Cloos MA, Knoll F, Zhao T, et al. Multiparametric imaging with heterogeneous radiofrequency fields. Nat. Commun 2016;7 doi: 10.1038/ncomms12445.
24. Zhang T, Pauly JM, Levesque IR. Accelerating parameter mapping with a locally low rank constraint. Magn. Reson. Med 2015;73:655–661 doi: 10.1002/mrm.25161. [PubMed: 24500817]
25. Wang X, Roeloffs V, Klosowski J, et al. Model-based T_1 mapping with sparsity constraints using single-shot inversion-recovery radial FLASH. Magn. Reson. Med 2018;79:730–740 doi: 10.1002/mrm.26726. [PubMed: 28603934]

26. Christodoulou AG, Shaw JL, Nguyen C, et al. Magnetic resonance multitasking for motion-resolved quantitative cardiovascular imaging. Nat. Biomed. Eng 2018;2:215–226 doi: 10.1038/s41551-018-0217-y. [PubMed: 30237910]
27. Li Z, Fu Z, Keerthivasan M, et al. Rapid high-resolution volumetric T1 mapping using a highly accelerated stack-of-stars Look Locker technique. Magn. Reson. Imaging 2021;79:1–10 doi: 10.1016/j.mri.2021.03.003. [PubMed: 33652063]
28. Li Z, Bilgin A, Johnson K, et al. Rapid high-resolution T1 mapping using a highly accelerated radial steady-state free-precession technique. J. Magn. Reson. Imaging 2019;49:239–252 doi: 10.1002/JMRI.26170. [PubMed: 30142230]
29. Piccini D, Feng L, Bonanno G, et al. Four-dimensional respiratory motion-resolved whole heart coronary MR angiography. Magn. Reson. Med 2017;77:1473–1484 doi: 10.1002/mrm.26221. [PubMed: 27052418]
30. Zhao B, Lu W, Hitchens TK, Lam F, Ho C, Liang ZP. Accelerated MR parameter mapping with low-rank and sparsity constraints. Magn. Reson. Med 2015;74:489–498 doi: 10.1002/mrm.25421. [PubMed: 25163720]
31. Doneva M, Börnert P, Eggers H, Stehning C, Sénégas J, Mertins A. Compressed sensing reconstruction for magnetic resonance parameter mapping. Magn. Reson. Med 2010;64:1114–1120 doi: 10.1002/mrm.22483. [PubMed: 20564599]
32. Lee D, Jin KH, Kim EY, Park S-H, Ye JC. Acceleration of MR parameter mapping using annihilating filter-based low rank hankel matrix (ALOHA). Magn. Reson. Med 2016;76:1848–1864 doi: 10.1002/MRM.26081. [PubMed: 26728777]
33. Maier O, Schoormans J, Schloegl M, et al. Rapid T1 quantification from high resolution 3D data with model-based reconstruction. Magn. Reson. Med 2019;81:2072–2089 doi: 10.1002/MRM.27502. [PubMed: 30346053]
34. Yaman B, Weingartner S, Kargas N, Sidiropoulos ND, Akcakaya M. Low-Rank Tensor Models for Improved Multidimensional MRI: Application to Dynamic Cardiac T_1 Mapping. IEEE Trans. Comput. Imaging 2019;6:194–207 doi: 10.1109/TCI.2019.2940916. [PubMed: 32206691]
35. Velikina J V, Alexander AL, Samsonov A. Accelerating MR parameter mapping using sparsity-promoting regularization in parametric dimension. Magn. Reson. Med 2013;70:1263–1273 doi: 10.1002/MRM.24577. [PubMed: 23213053]
36. Feng L, Liu F, Soultanidis G, et al. Magnetization-prepared GRASP MRI for rapid 3D T1 mapping and fat/water-separated T1 mapping. Magn. Reson. Med 2021;86:97–114 doi: 10.1002/mrm.28679. [PubMed: 33580909]
37. Deichmann R.Fast high-resolution T1 mapping of the human brain. Magn. Reson. Med 2005;54:20–27 doi: 10.1002/MRM.20552. [PubMed: 15968665]
38. Feng L, Wen Q, Huang C, Tong A, Liu F, Chandarana H. GRASP-Pro: imProving GRASP DCE-MRI through self-calibrating subspace-modeling and contrast phase automation. Magn. Reson. Med 2020;83:94–108 doi: 10.1002/mrm.27903. [PubMed: 31400028]
39. Benkert T, Tian Y, Huang C, DiBella EVR, Chandarana H, Feng L. Optimization and validation of accelerated golden-angle radial sparse MRI reconstruction with self-calibrating GRAPPA operator gridding. Magn. Reson. Med 2018;80:286–293 doi: 10.1002/mrm.27030. [PubMed: 29193380]
40. Feng L, Huang C, Shanbhogue K, Sodickson DK, Chandarana H, Otazo R. RACER-GRASP: Respiratory-weighted, aortic contrast enhancement-guided and coil-unstreaking golden-angle radial sparse MRI. Magn. Reson. Med 2018;80:77–89 doi: 10.1002/mrm.27002. [PubMed: 29193260]
41. Captur G, Gatehouse P, Keenan KE, et al. A medical device-grade T1 and ECV phantom for global T1 mapping quality assurance—the T 1 Mapping and ECV Standardization in cardiovascular magnetic resonance (T1MES) program. J. Cardiovasc. Magn. Reson. 2016 181 2016;18:1–20 doi: 10.1186/S12968-016-0280-Z.
42. Chung S, Kim D, Breton E, Axel L. Rapid B1+ mapping using a preconditioning RF pulse with TurboFLASH readout. Magn. Reson. Med 2010;64:439–446 doi: 10.1002/MRM.22423. [PubMed: 20665788]
43. Lin LI-K. A Concordance Correlation Coefficient to Evaluate Reproducibility. Biometrics 1989;45:255 doi: 10.2307/2532051. [PubMed: 2720055]

44. Captur G, Bhandari A, Brühl R, et al. T 1 mapping performance and measurement repeatability: results from the multi-national T 1 mapping standardization phantom program (T1MES). J. Cardiovasc. Magn. Reson. 2020 221 2020;22:1–17 doi: 10.1186/S12968-020-00613-3.

45. Jiang Y, Ma D, Keenan KE, Stupic KF, Gulani V, Griswold MA. Repeatability of magnetic resonance fingerprinting T1 and T2 estimates assessed using the ISMRM/NIST MRI system phantom. Magn. Reson. Med 2017;78:1452–1457 doi: 10.1002/MRM.26509. [PubMed: 27790751]

46. Jang J, Ngo LH, Captur G, Moon JC, Nezafat R. Measurement reproducibility of slice-interleaved T1 and T2 mapping sequences over 20 months: A single center study. PLoS One 2019;14:e0220190 doi: 10.1371/JOURNAL.PONE.0220190.

47. Zhou R, Weller DS, Yang Y, et al. Dual-excitation flip-angle simultaneous cine and T1 mapping using spiral acquisition with respiratory and cardiac self-gating. Magn. Reson. Med 2021;86:82–96 doi: 10.1002/MRM.28675. [PubMed: 33590591]

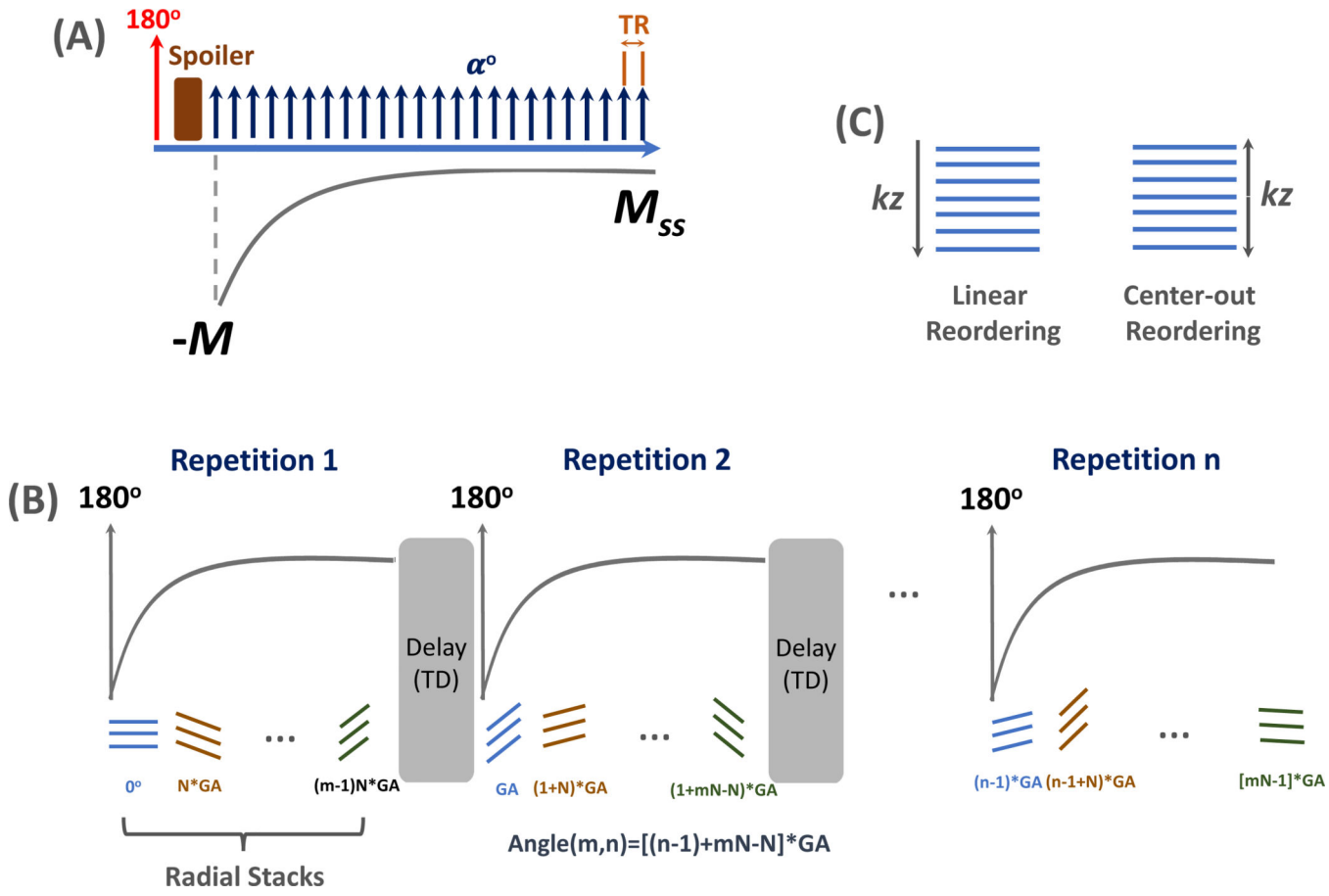

Figure 1.

(a) Magnetization evolution after an IR (inversion recovery) preparation in Look-Locker acquisition. With constant RF excitation, magnetization starts from -*M* and reaches a steady state indicated as *Mss*. (b) MP-GRASP acquisition scheme. Following each IR preparation, a series of continuous radial stacks are acquired. The acquisition ordering is designed in a way that all the spokes at a given rotation angle, referred to as a radial stack, is acquired before moving to the next rotation angle. A delay is added between different IR preparations to allow for magnetization recovery. The acquisition angle for each radial stack follows the equation shown below, where *m* indicates the m^{th} spoke, and *n* indicates the n^{th} repetition, and *N* indicates the total number of repetitions to be acquired. (c) The acquisition of each radial stack can be implemented with a linear reordering scheme (from one edge to the other side) or a center-out reordering scheme (from the center to the periphery).

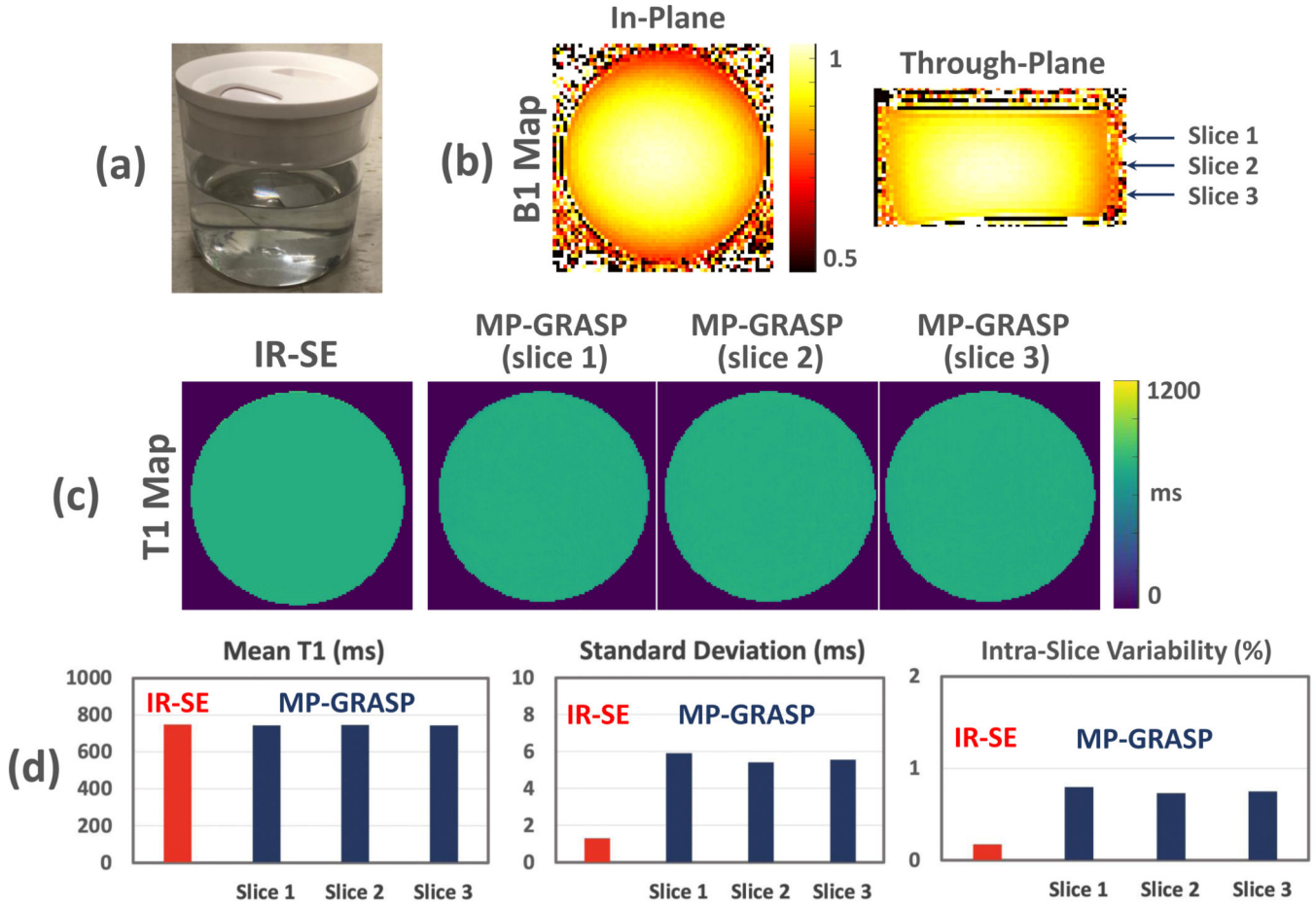

Figure 2.

(a) The single tube phantom filled with uniform $MnCl_2$ liquid. (b) 2D B1 maps for the single tube phantom imaging, one slice in axial plane and one slice in coronal plane. The arrows indicate the slice locations used for subsequent image analysis. (c) Comparison of T1 maps estimated from IR-SE (1 slice) and MP-GRASP (3 slices). The T1 maps are homogeneous visually, indicating that both methods can be robust to B1 variation. (d) MP-GRASP generated mean T1 values that are consistent with the IR-SE measurement. Although the IR-SE T1 map has a lower standard deviation compared to MP-GRASP, both methods yielded very low intra-slice variation (below 1%), indicating high repeatability.

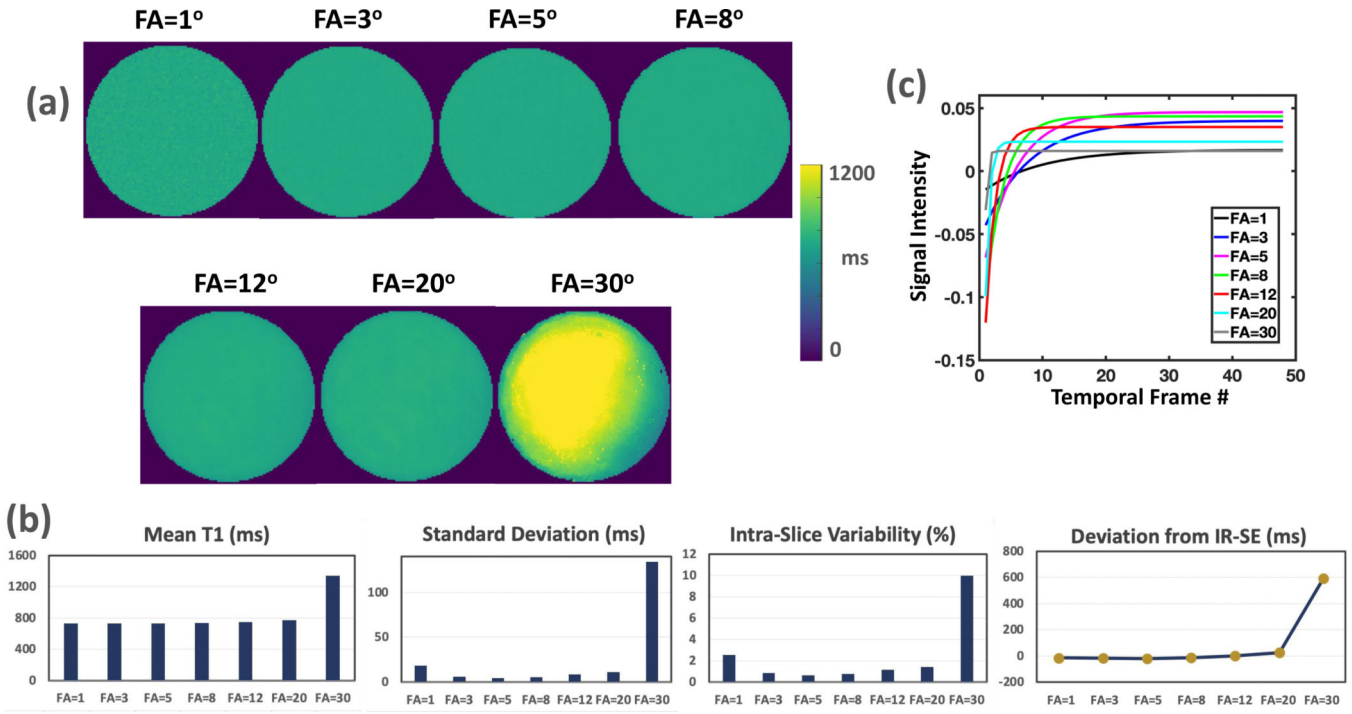

Figure 3.

(a) Comparison of MP-GRASP T1 maps estimated with different flip angles. The mean T1 value estimated from flip angle of 1° is noisy because of the low signal. (b) Quantitative comparison of mean T1 values estimated from (a). Consistent mean T1 values can be obtained with different flip angles up to 20°. The standard deviation and intra-slice repeatability indicate that the T1 map from the flip angle of 5° (an angle close to the Ernst angle) is the best. On the other side, the mean T1 value estimated from flip angle of 30° has larger deviation from the reference, which is because of the flattening of T1 recovery curve (loss of T1 recovery range) in Look-Locker acquisition as shown in (c).

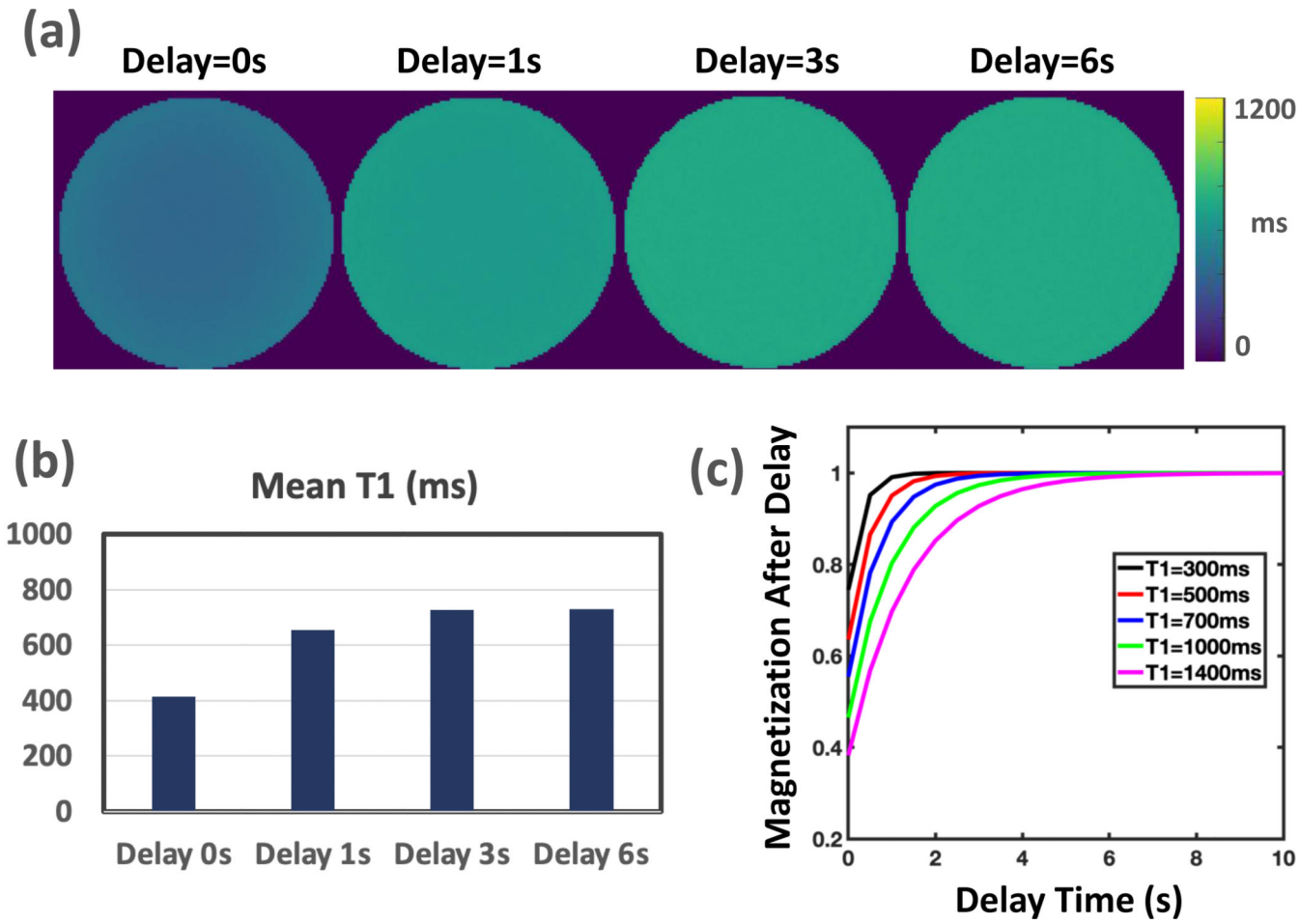

Figure 4.

(a) Comparison of MP-GRASP T1 maps acquired with different delay times. Insufficient delay time prevents full signal recovery before a new IR preparation, thus resulting T1 estimation errors. (b) Quantitative comparison of mean T1 values estimated from (a). (c) A numerical simulation to investigate the delay time needed for different T1 values to be estimated in standard Look-Locker imaging. It indicates that with the increase of underlying T1 values, the delay time also needs to be increased to ensure accurate T1 estimation.

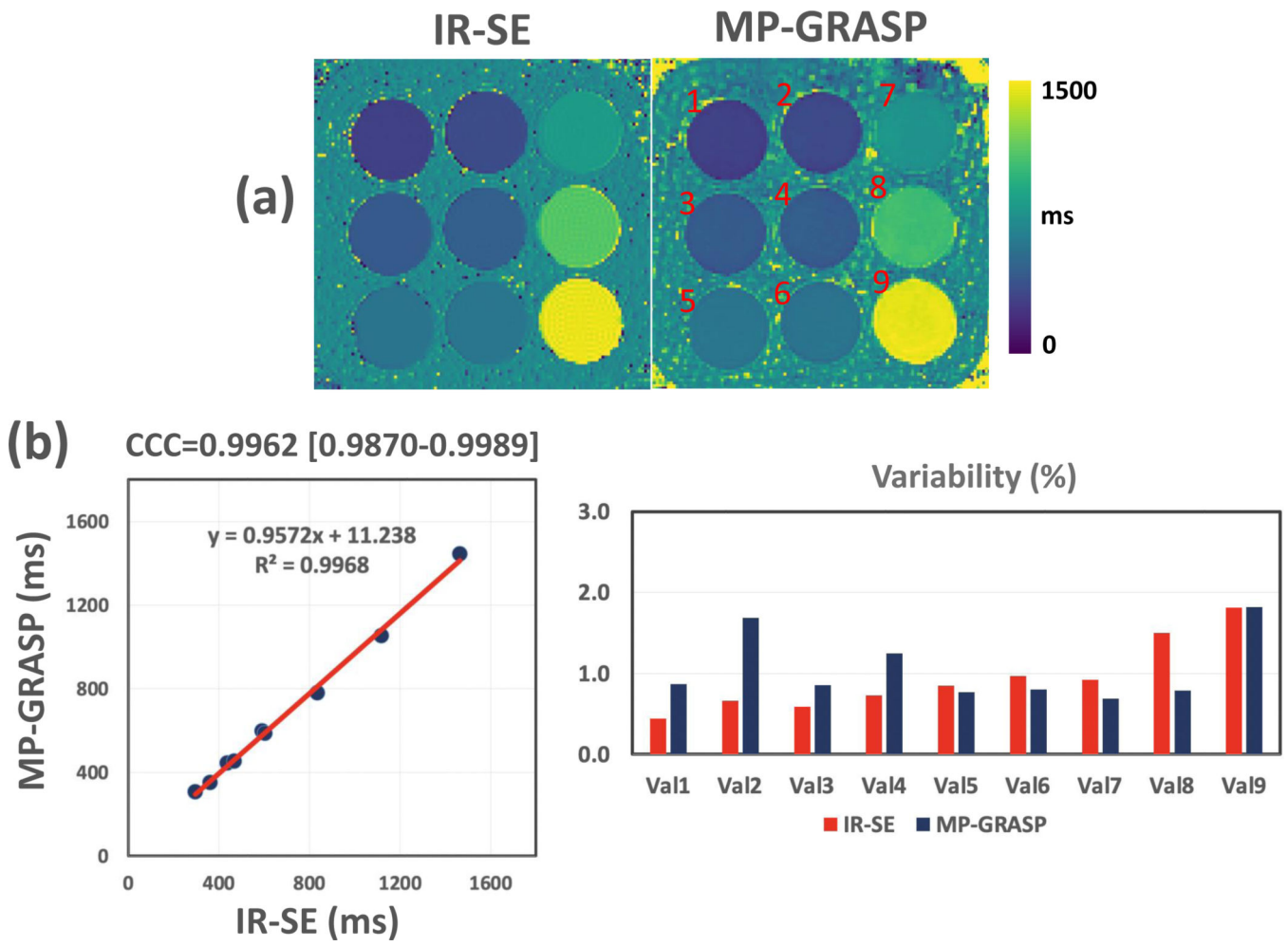

Figure 5.

(a) Comparison of one slice of T1 map estimated from IR-SE and MP-GRASP imaging. (b) The linear correlation shows a strong correlation between the mean T1 values estimated from the two methods, and the Lin's CCC was 0.9962 (95% confidence interval= 0.9870 to 0.9989). The variability of T1 estimation over all the 12 scans is good (below 2% for all phantom vials) for both IR-SE and MP-GRASP.

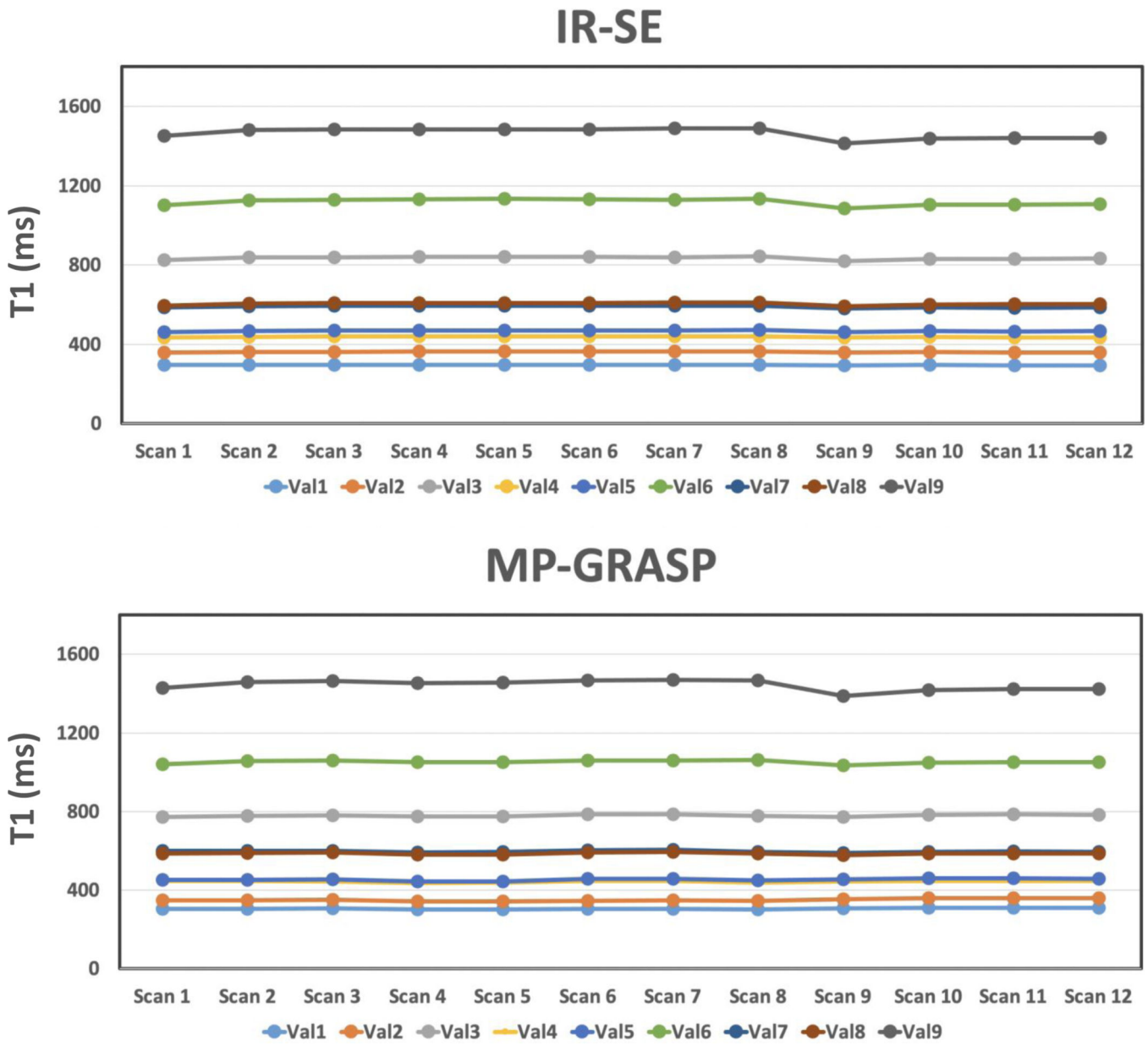

Figure 6.

Comparison of mean T1 values estimated from each phantom vial from MP-GRASP and IR-SE imaging performed in two settings. In the first setting, MR scans started 3 hours after the phantom was put into the scanner. MP-GRASP and IR-SE were alternatively scanned for a total of 8 times each (referred to as Scan 1 to Scan 8). In the second setting, MRI scans started right after the phantom was put into the scanner, and MP-GRASP and IR-SE were alternatively scanned for a total of 4 times each (referred to as Scan 9 to Scan 12). For each setting, the T1 estimation is repeatable. However, for vials with larger T1 values (e.g., vial 7 to vial 9), there is a jump of measured T1 value from the first scan (Scan 1 and Scan 9) to the rest, which is potentially due to adjustment of temperature in the beginning, and this trend was observed both in the IR-SE and the MP-GRASP results. In addition, potentially

due to fluctuation of scanner room temperature in different days, the T1 values estimated in the second setting are generally lower compared to that from the first setting, and this was also observed both in the IR-SE and the MP-GRASP results.

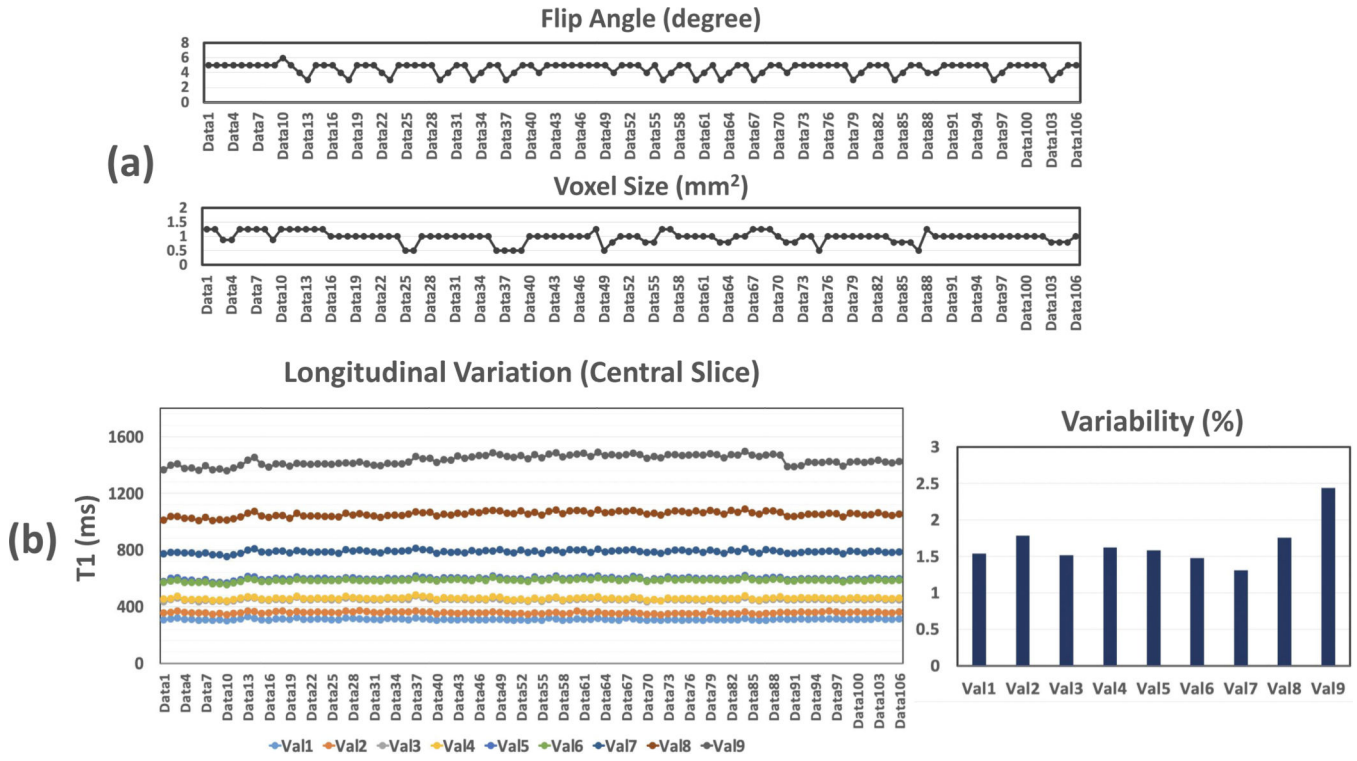

Figure 7.

The longitudinal variations of mean T1 values over all the 106 datasets for a central slice of T1 map, along with corresponding variation of flip angle and voxel size. Similar results for the peripheral slice are shown in Supporting Information Figure S1. Different line colors indicate different phantom vials. The longitudinal repeatability of T1 estimation is also shown in the figure. The variation of T1 measurement was below 2% for vials 1–8, and it was slightly larger for vial 9, which is still below 2.5%. For phantom vial 8 and vial 9, there is slight increase and then decrease of mean T1 values along time, which is consistent with the trend observed in Figure 6.

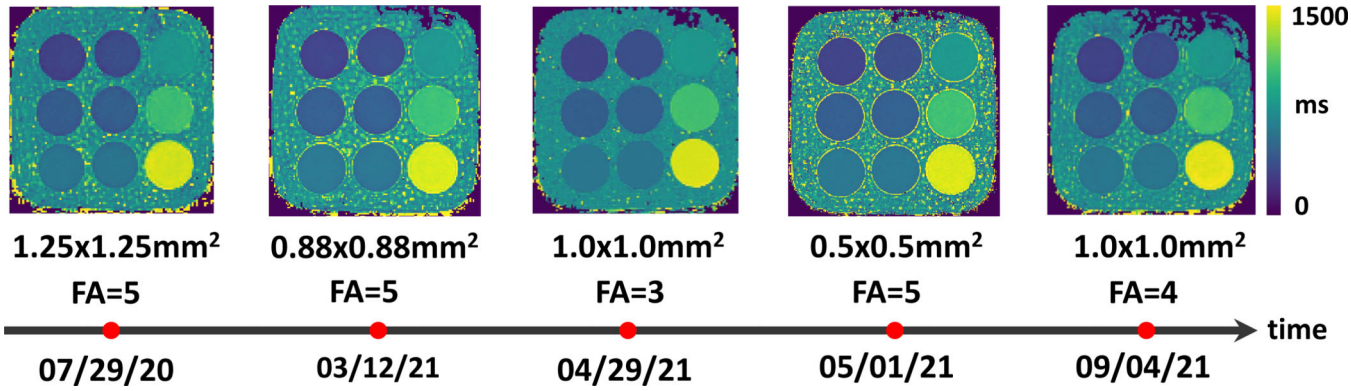

Figure 8.

Representative MP-GRASP T1 maps from the T1MES phantom at different time points. Despite different imaging parameters, the T1 maps are visually consistent for all phantom vials.

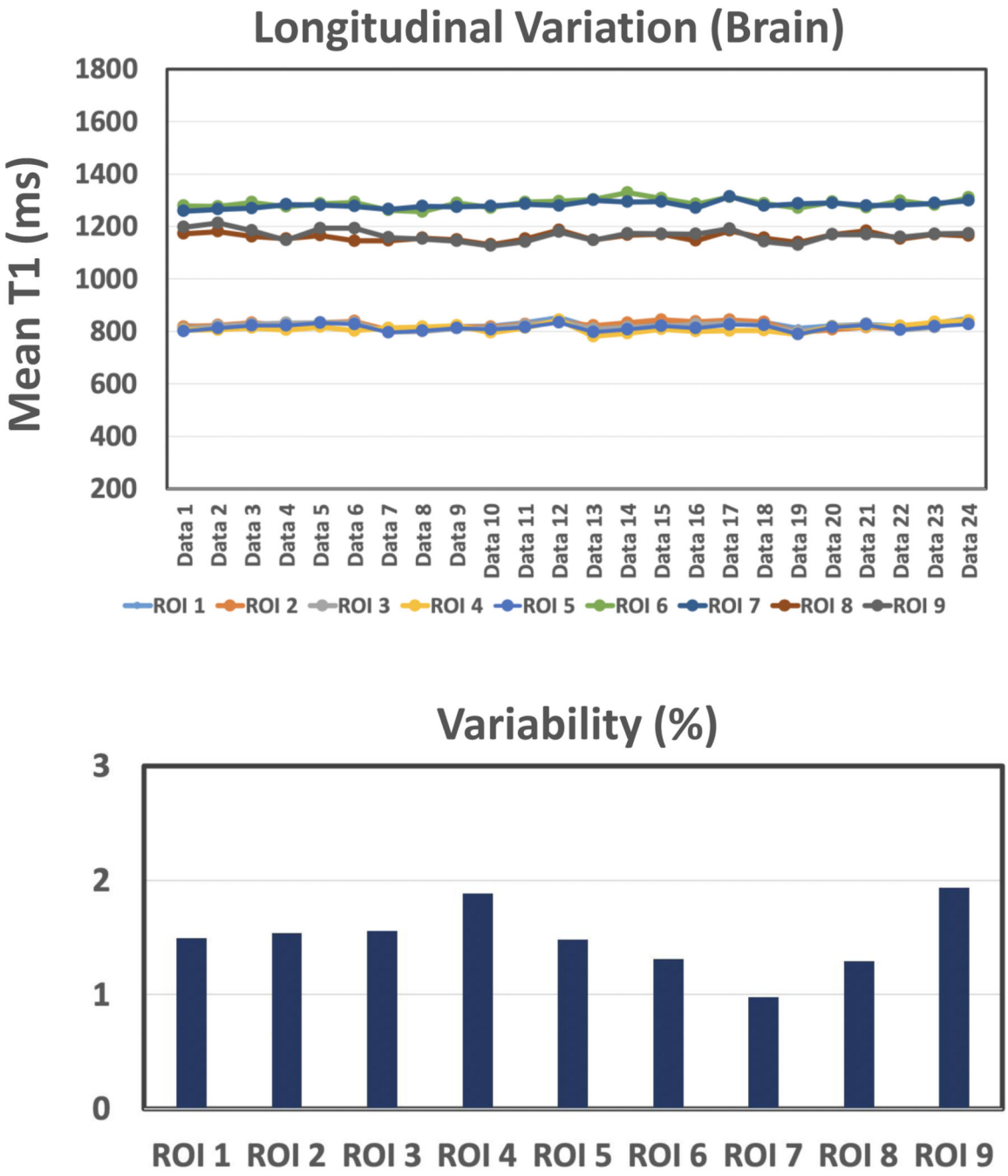

Figure 9.

Dynamic variations of MP-GRASP T1 values over all the 24 brain datasets for all the 9 selected ROIs. The variation of T1 measurement s below 2% in all ROIs, which suggests good repeatability of T1 mapping using MP-GRASP in the brain.

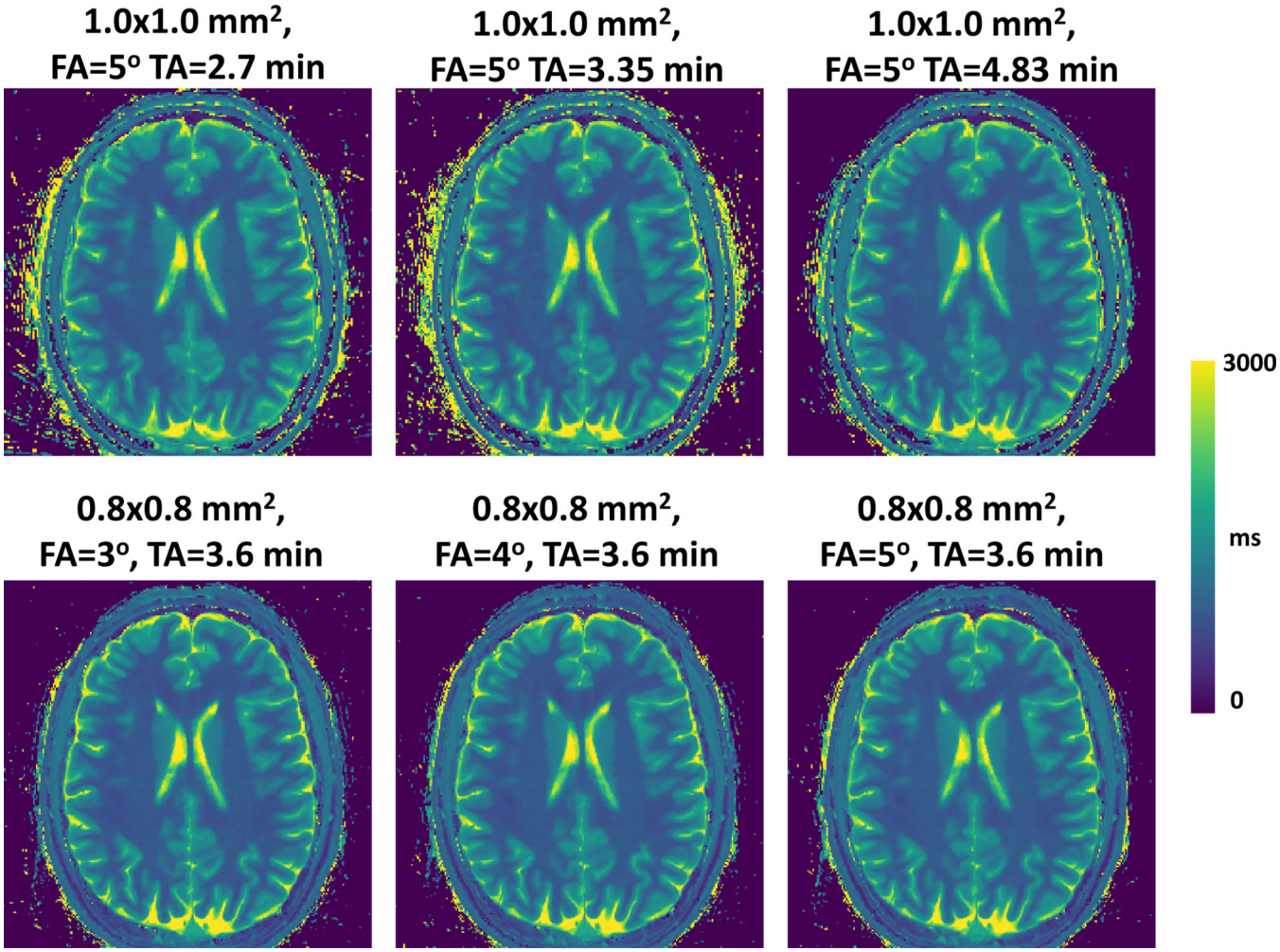

Figure 10.

One slice of brain T1 map acquired with different flip angles, acquisition times and spatial resolution. On the top row, the T1 maps were acquired with an in-plane spatial resolution of 1.0×1.0 mm^2, flip angle of 5°, and different acquisition times/acceleration rates. For the bottom row, the T1 maps were acquired using different flip angles but the same spatial resolution (0.8×0.8 mm^2) and acquisition time. Overall, the brain T1 maps from different imaging protocols are visually consistent.